ChemPubSoc Europe

DOI: 10.1002/celc.201500455

CHEMELECTROCHEM Communications

Synthesis and Electrochemistry of $Na_{2.5}(Fe_{1-y}Mn_y)_{1.75}(SO_4)_3$ Solid Solutions for Na-Ion Batteries

Suhao Wei,[a] Benoit Mortemard de Boisse,[a, b] Gyosuke Oyama,[a] Shin-ichi Nishimura,[a, b] and Atsuo Yamada*[a, b]

$Na_{2+2x}Fe_{2-x}(SO_4)_3$ was recently reported as a promising cathode material for Na-ion batteries with high voltage generation (3.8 V vs. Na/Na^+), high energy density, and extreme high-rate operation, making it competitive to lithium battery cathodes. Following our identification of the narrow off-stoichiometric region in $Na_{2+2x}Fe_{2-x}(SO_4)_3$ solid solutions (x around 0.25), we report here the effect of Mn substitution in $Na_{2.5}(Fe_{1-y}Mn_y)_{1.75}(SO_4)_3$ ($y=0$, 0.25, 0.5, 0.75, and 1.0) solid solutions when increasing the voltage of the Fe^{3+}/Fe^{2+} redox couple, but with a simple capacity decrease, owing to the entire Mn^{2+} inactivity.

Lithium-ion and sodium-ion batteries were intensively studied in the 1980s to power mobile communication devices. However, with the commercialization of the first Li-ion battery in the early 1990s, most efforts on Na-ion battery research shifted to lithium-ion batteries, as sodium-ion batteries could not compete for high-energy-density applications, owing to the larger size and heavier weight of Na^+.

Nowadays, the world faces a new energetic challenge. Transition towards green energy sources is required, but remains a utopia as the energy produced in solar and wind farms is intermittent. To overcome this issue, it is necessary to set up power grids that are able to compensate energetic fluctuations by using large-scale stationary batteries. Although the few resources and high price of Li limits the application of Li-ion batteries in this field, Na-ion batteries represent one the best candidates, owing to the price and abundance of the raw materials[1] and to the fast bulk diffusion as well as low interfacial kinetic barrier of Na^+.[2]

Given that energy density is not a critical limitation factor, the Na-ion technology, set aside for two decades, has been (re)investigated since the 2000s. Among the various positive electrode materials recently reported, many are based on Fe/Mn redox centers as the ultimate elemental strategy. They consist of layered oxides[3] or polyanionic materials such as phosphates,[4] pyrophosphates,[5] fluorophosphates,[6] and so forth.

Following recent research on sulfate-based polyanionic materials in Li-ion batteries,[7] our group reported the synthesis and electrochemical properties of kröhnkite $Na_2Fe(SO_4)_2.2H_2O$[8] and alluaudite $Na_{2+2x}Fe_{2-x}(SO_4)_3$ ($0.25 \leq x \leq 0.3$).[9] The latter shows highest Fe^{3+}/Fe^{2+} redox couple voltage ever reported (3.8 V vs. Na/Na^+, and hence 4.1 V vs. Li/Li^+), associated with good discharge capacity (100 $mAh\,g^{-1}$at C/20) and rate capability (60% are still available at 20C rate). Moreover, its high energy density (> 540 $Wh\,g^{-1}$) could make Na-ion batteries competitive with state of the art lithium-ion cells.[9a]

In this work, we focus on the substitution of Fe by Mn to form $Na_{2.5}(Fe_{1-y}Mn_y)_{1.75}(SO_4)_3$ ($y=0$, 0.25, 0.5, 0.75, and 1.0) solid solutions. Our goal is to study the impact of the substitution on the structural, electrochemical, and redox properties and to identify the similarities and differences with the other polyanionic cathode materials. We expect the observation of the Mn^{3+}/Mn^{2+} redox couple around 4.5 V versus Na/Na^+ as well as a significant increase in the Fe^{3+}/Fe^{2+} potential.[10]

The structure of alluaudite $Na_{2+x}Fe_{2-x}(SO_4)_3$ has been reported previously.[9a,c] In this structure, Fe^{2+} ions are located in octahedral sites sharing edges with the nearest neighbor, creating Fe_2O_{10} dimers. Fe_2O_{10} dimers are, in turn, bridged together by sharing corners with SO_4 tetrahedrons, creating a three-dimensional framework with large tunnels along the c axis. Na^+ ions occupy three different sites in these tunnels, one fully occupied and two partially occupied.[9a] In the case of off-stoichiometric $Na_{2.5}Fe_{1.75}(SO_4)_3$, the unfilled part of the Fe site is occupied by Na^+ ions.[9c]

Figure 1 shows the XRD patterns of the as-prepared $Na_{2.5}(Fe_{1-y}Mn_y)_{1.75}(SO_4)_3$ ($y=0$, 0.25, 0.5, and 0.75) solid solutions and of $Na_{2.6}Mn_{1.7}(SO_4)_3$ (hereafter denoted as "$y=1$" for clarity purposes). The increasing shift of the peaks to lower 2θ angles with increasing Mn content suggests an increase in the cell parameters and the volume, as a result of the larger Mn^{2+} ion ($r_i=0.83$ Å) compared to Fe^{2+} ($r_i=0.61$ Å).[11]

We then carried out Rietveld refinements (Figure S1 and Table S1) assuming that the solid solutions crystallize in the alluaudite structure. The evolution of the refined cell parameters is given in Figure 2 and confirm the increasing volume of the cell with increasing Mn content.

The good quality of the fittings given by the R_{wp} and R_B reliability factors indicates the efficient substitution of Fe by Mn in the $Na_{2.5}(Fe_{1-y}Mn_y)_{1.75}(SO_4)_3$ ($y=0$, 0.25, 0.5, 0.75, and 1) solid solutions, as expected from the recent conclusions by

[a] S. Wei,[+] Dr. B. Mortemard de Boisse,[+] G. Oyama, Dr. S. Nishimura, Prof. A. Yamada
Department of Chemical Engineering
The University of Tokyo
7-3-1 Hongo, Bunkyo-ku, Tokyo 113-8656 (Japan)
E-mail: yamada@chemsys.t.u-tokyo.ac.jp

[b] Dr. B. Mortemard de Boisse,[+] Dr. S. Nishimura, Prof. A. Yamada
Unit of Elements Strategy Initiative for Catalysts & Batteries (ESICB)
Kyoto University, Kyoto 615-8510 (Japan)

[+] These authors contributed equally to this work

Supporting Information for this article is available on the WWW under http://dx.doi.org/10.1002/celc.201500455.

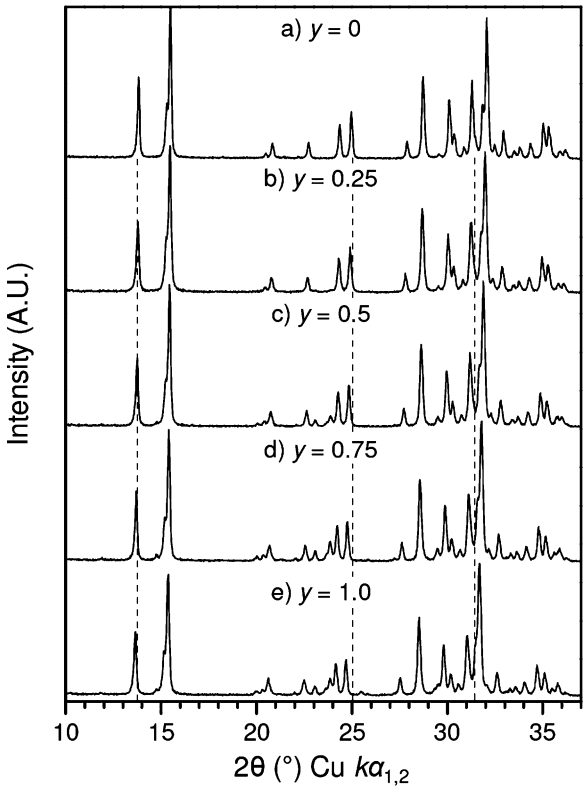

Figure 1. XRD patterns of the a) $y=0$, b) $y=0.25$, c) $y=0.5$, d) $y=0.75$, and e) $y=1$ $Na_{2.5}(Fe_{1-y}Mn_y)_{1.75}(SO_4)_3$ solid solutions. The grey dashed lines highlight the shift of the diffraction peaks towards lower 2θ values as the Mn content increases.

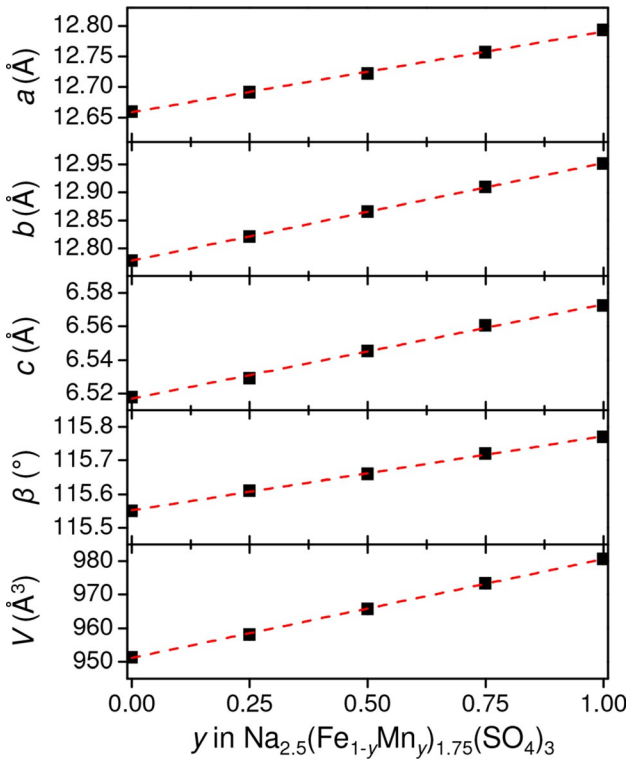

Figure 2. Evolution of the cell parameters and of the volume in the $Na_{2.5}(Fe_{1-y}Mn_y)_{1.75}(SO_4)_3$ solid solutions. The red dashed lines show the linear evolution of the various parameters with the Mn content (linear fittings).

Dwibedi's et al. on the isostructural $Na_{2.4}Fe_{1.8}(SO_4)_3$ and $Na_{2.44}Mn_{1.79}(SO_4)_3$ compounds.[12] By closely looking at the indexation of the diffraction patterns (Figure S1), we observe that the alluaudite phase does not allow perfect matching of the XRD patterns, and some impurities must be included: Fe_3O_4 [$Na_{2.5}Fe_{1.75}(SO_4)_3$ sample] or $Na_2Mn_3(SO_4)_4$ (Mn containing samples). The structure of the latter will be published in a forthcoming paper. The number of impurities increases from 0.8 to 8.3% with increasing Mn content (Table S1).

The electrochemical properties of the different $Na_{2.5}(Fe_{1-y}Mn_y)_{1.75}(SO_4)_3$ ($y=0$, 0.25, 0.5, 0.75, and 1) solid solutions were investigated in Na cells. The galvanostatic curves recorded at C/20 between 2.5 and 4.4 V are given in Figures 3 a–e. The first cycle is highlighted in red.

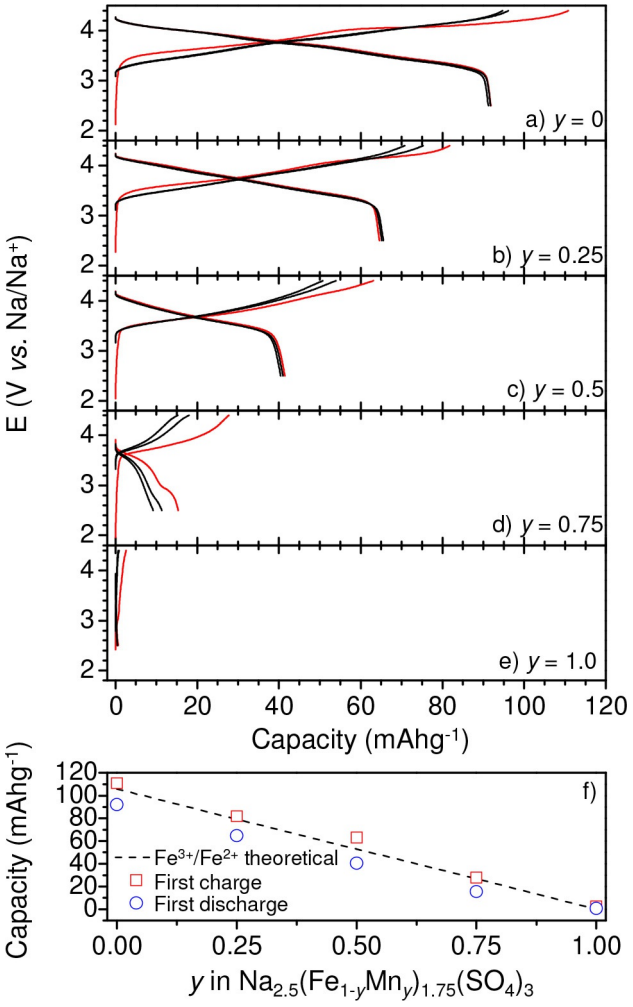

Figure 3. Galvanostatic cycling curves recorded between 2.5 and 4.4 V at C/20 with Na/$NaClO_4$ in propylene carbonate (1 M)/$Na_{2.5}(Fe_{1-y}Mn_y)_{1.75}(SO_4)_3$ cells: a) $y=0$, b) $y=0.25$, c) $y=0.5$, d) $y=0.75$, and e) $y=1.0$. f) Evolution of the first charge and discharge capacities are reported on along with the theoretical capacity, solely based on the Fe^{3+}/Fe^{2+} activity.

As one can see, partial substitution of Fe by Mn reduces the first charge capacity from 110 mAh g^{-1} ($y=0$) to 80 ($y=0.25$), 60 ($y=0.5$), 30 ($y=0.75$), and 0 mAh g^{-1} ($y=1$). This collapse is highlighted in Figure 3 f, which also shows that the obtained

capacity corresponds to the theoretical one, assuming the activity of Fe^{3+}/Fe^{2+} only. One can see in this result the entire inactivity of the Mn^{3+}/Mn^{2+} redox couple, as also observed in $Li_2(Fe_{1-y}Mn_y)P_2O_7$ solid solutions ($0 \leq y \leq 1$)[10] and, more recently, in $Na_{2.44}Mn_{1.79}(SO_4)_3$.[12]

We then plotted the d*Q*/d*E* curves, corresponding to the derivative of the current with respect to the voltage, for the $y=$ 0, 0.25, 0.5, and 0.75 solid solutions, as shown in Figures 4a and 4b for the first and second cycles, respectively. As one can see, the first charge profile shows two oxidation peaks, whereas three peaks are observed in the consecutive discharge and cycles (each peak corresponding to a given Na site). This evolution in the electrochemical profile is ascribed to structural changes occurring during the first charge[9a] and will be published in a forthcoming paper.

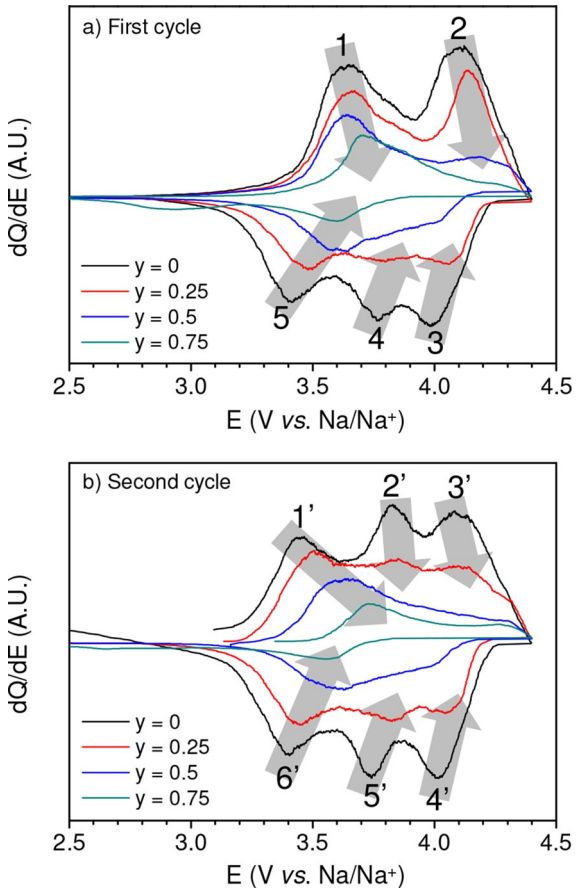

Figure 4. d*Q*/d*V* plots of the a) first and b) second cycles of the $Na_{2.5}(Fe_{1-y}Mn_y)_{1.75}(SO_4)_3$ solid solutions ($y=0$, 0.25, 0.5, and 0.75). The grey arrows highlight the shift of the various peaks to higher voltages.

It can be seen that the relative intensity of the second peak of the first charge decreases as the Mn content increases. This is explained by the Mn^{2+} inactivity that lowers the amount of Na^+ ions to be extracted by the Fe^{3+}/Fe^{2+} redox process. For the $y=0.5$ solid solution, peak 1 represents the predominant contribution with a large decrease in the peak 2 signal; for the $y=0.75$ solid solution, the de-sodiation process does not show any contribution from peak 2. A lesser contribution of peak 2 affects the subsequent high voltage signals of peaks 3, 4, 2′, 3′, 4′, and 5′ whose relative intensity diminishes as the Mn content increases.

As highlighted by the grey arrows in Figure 4, the voltage at which each (de)intercalation occurs is shifted to higher values as the Mn content increase. Such a phenomenon is known to be correlated to the higher Gibbs free energy of the charged state.[13] Upon charge, the $M^{2+} \rightarrow M^{3+}$ reaction is accompanied by de-sodiation (delithiation), and the formed sodium (lithium) vacancies stabilize the higher oxidation state of the M^{3+} cation.[13] Here, however, the Mn^{2+} ions that are stabilized by nearby Na^+ ions are not involved in the redox reaction. This makes the formation of Na^+ vacancies unfavorable around the Mn^{2+} and Fe^{3+} ions and results in local frustrations that increase the Gibbs free energy of the charged state, thus increasing the potential of the Fe^{3+}/Fe^{2+} redox couple. Also, it must be noted that Fe^{3+} migration upon charge would be suppressed by the smaller capacity in the Mn-substituted samples, maintaining the Fe^{3+}– Fe^{3+} repulsive local interactions and, hence, high-voltage operation after the first cycle. Such a phenomenon was already observed in $Li_2M_xFe_{1-x}P_2O_7$ solid solutions (M = Mn, Co, Mg).[13b]

To further understand the effect of Mn on the redox properties, we conducted ^{57}Fe Mössbauer spectroscopy and a X-ray absorption near-edge spectroscopy (XANES) study of the mate-

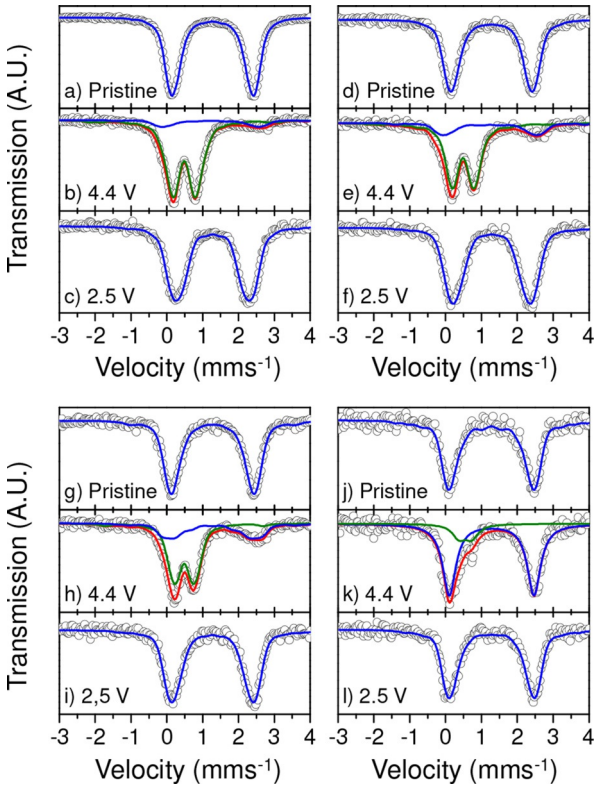

Figure 5. ^{57}Fe Mössbauer spectra of the $Na_{2.5}(Fe_{1-y}Mn_y)_{1.75}(SO_4)_3$ solid solutions in their pristine, charged (4.4 V), and discharged (2.5 V) states: a, b, c) $y=0$, d, e, f) $y=0.25$, g, h, i) $y=0.5$ and j, k, l) $y=0.75$. Black circles: observed; blue line: Fe^{2+} site; green line: Fe^{3+} site; red line: calculated when two sites are involved.

rials in the pristine, charged, and discharged states. Figure 5 shows the ^{57}Fe Mössbauer spectra of the pure-iron and Mn-substituted samples. The spectra of the pristine materials all exhibit a quadrupole doublet that can be fitted by using one iron site whose isomer shift ($\delta \approx 1.28$ mm s^{-1}) is similar to that of α-$Fe^{II}SO_4$ (Fe^{2+} ions in octahedral FeO_6 environment created by SO_4^{2-} anions). Distribution fittings using a fixed FWHM value (0.25 mm s^{-1}) were carried out to take into account the distribution of environments around the Fe probe atom. The Mössbauer parameters are reported in Table S2. The increasing value of the quadrupole splitting with the Mn content [from $\Delta^* = 2.20(1)$ to $\Delta^* = 2.33(1)$ mm s^{-1}] indicates a larger electric field gradient at the Fe nuclei, as the Mn^{2+} ions are more involved in the M_2O_{10} dimers, randomly distorting the FeO_6 octahedron with which it shares oxygen atoms. The spectra of the charged materials show a new signal whose isomer shift ($\delta \approx 0.5$ mm s^{-1}) is similar to that of $Fe_2^{III}(SO_4)_3$ (Fe^{3+} ions in octahedral FeO_6 environments created by SO_4^{2-} anions). This new signal confirms the $Fe^{2+} \rightarrow Fe^{3+}$ redox process upon charge.

As one can see, a significant portion of the Fe^{2+} ions remain unoxidized in the 4.4 V charged state, creating a gap in the electrochemical results (Figure 3 f). Such a contradiction is not uncommon and results from the electrolyte decomposition when the cutoff voltage is set greater than 3.5 V versus Na/Na^+.[14]

For the samples charged to 4.4 V, the overall decrease in the quadrupole splitting of the Fe^{2+} and Fe^{3+} sites indicates a decrease in the disorder with Mn content. As fewer Fe^{2+} ions can be oxidized and more Mn^{2+} ions are present, it becomes highly probable for Fe^{2+} ions to be located in $Fe^{2+}Mn^{2+}O_{10}$ dimers, whereas samples with lower Mn contents show various possible environments ($Fe^{2+}Mn^{2+}O_{10}$, $Fe^{3+}Mn^{2+}O_{10}$, $Fe^{2+}Fe^{2+}O_{10}$, $Fe^{2+}Fe^{3+}O_{10}$). Upon consecutive discharge, only one signal corresponding to Fe^{2+} ions ($\delta \approx 1.28$ mm s^{-1}) is observed, indicating the reversibility of the $Fe^{2+} \rightarrow Fe^{3+}$ redox process for all materials.

Finally, we investigated the redox contribution of the Mn^{2+} by conducting XANES measurements on a $Na_{2.4-x}Mn_{0.72}Fe_{1.08}(SO_4)_3$ sample. The XANES spectra recorded at the Fe and Mn *K*-edges for the pristine, charged, and discharged states are shown in Figure 6. Upon charge, the Fe *K*-edge (Figure 6 a) shifts to higher energy values, confirming the $Fe^{2+} \rightarrow Fe^{3+}$ redox process that was observed by ^{57}Fe Mössbauer spectroscopy. Upon discharge, the process is fully reversible, as shown by the overlap with the spectrum of the pristine material. On the other hand, the Mn *K*-edge spectra (Figure 6 b) do not show any evolution between the pristine, charged, and discharged states, confirming that the Mn^{2+} ions are inactive during cycling. Such inactivity, or much less activity than Fe, is common in polyanionic compounds[10] and may result from the high voltage of the Mn^{3+}/Mn^{2+} redox couple in the alluaudite phases.[12] The use of an electrolyte that is stable at high voltage is required before we can conclude on this topic.

To summarize, by using a low-temperature solid-state reaction and very anhydrous synthesis conditions, we showed the existence of a complete solid solution of $Na_{2.5}(Fe_{1-y}Mn_y)_{1.75}(SO_4)_3$ ($0 \leq y \leq 1$). Mn substitution in $Na_{2.5}(Fe_{1-y}Mn_y)_{1.75}(SO_4)_3$ increases the voltage of the Fe^{3+}/Fe^{2+} redox couple, but unfortunately leads to simple decrease of the discharge capacity, owing to the Mn^{3+}/Mn^{2+} inactivity that makes $Na_{2+2x}Fe_{2-x}(SO_4)_3$ the best candidate among the alluaudite $Na_{2+x}M_{2-x}(SO_4)_3$ (M = transition metal) family for high-energy-density Na-ion batteries.

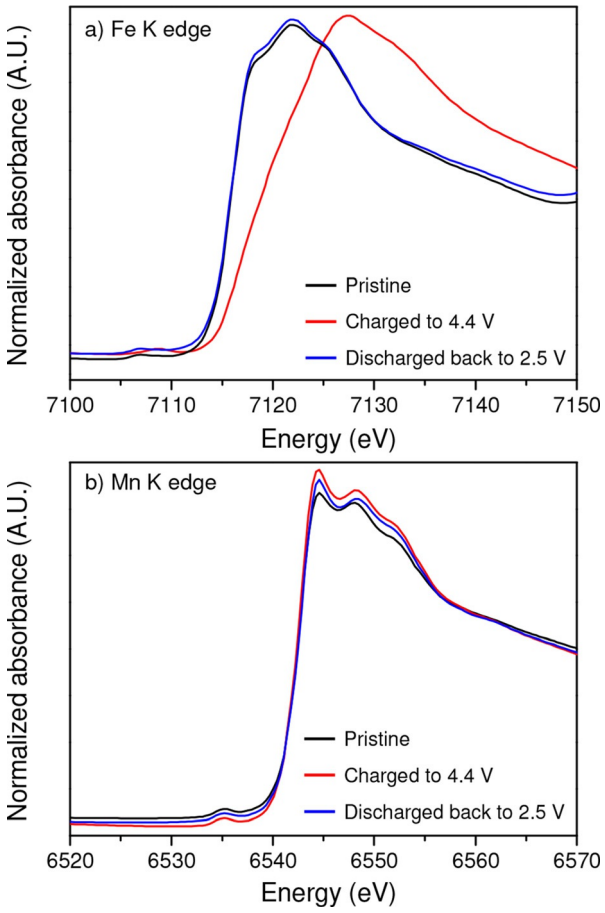

Figure 6. XANES spectra of the a) Fe and b) Mn *K*-edges of $Na_{2.4}Mn_{0.72}Fe_{1.08}(SO_4)_3$ in its pristine (black line), charged (red line), and discharged (blue line) states.

Experimental Section

The targeted materials were prepared by following the method previously reported[9a] from stoichiometric amounts of Na_2SO_4 (Wako, 99%), $MnSO_4$, and $FeSO_4$. $MnSO_4$ and $FeSO_4$ were prepared by separately annealing $MnSO_4.5H_2O$ (Wako, 99.9%) and $FeSO_4.7H_2O$ (Wako, 99%) under vacuum at 200 °C for 12 h. The anhydrous precursors were ground in a mortar under an Ar atmosphere and introduced in a ball-milling jar for further mixing for 4 h. Depending on the targeted material, 50 mL of acetone was added (Fe containing samples) or not (pure Mn sample) to prevent decomposition of $FeSO_4$. The resulting powder was then pressed into pellets and heat treated at 300 °C (pure Fe sample) or 350 °C (Mn containing samples) for 18 h under an Ar flow. This heat treatment was repeated with intermediate grinding. No increase in the weight of the pellets was measured after annealing, confirming the target composition.

X-ray powder diffraction (XRD) patterns were acquired in the 2θ range of 10–70° (0.02° step size) by using a Rigaku RINT-TTR-III diffractometer (operating at 300 mA, 50 kV) equipped with a CuKα source.

The samples were protected from environmental moisture by using specifically designed airtight sample holders. Rietveld refinements were performed by using TOPAS v3 (Bruker-AXS) software.

Electrochemical characterizations were carried out with Na/1 M $NaClO_4$ in propylene carbonate/$Na_{2.5}(Fe_{1-y}Mn_y)_{1.75}(SO_4)_3$ batteries assembled in 2032-type coin cells. Positive electrodes were a mixture of active material/acetylene black/polytetrafluoroethylene in an 85/10/5 weight ratio that were pressed (5 MPa, 30 s) onto an Al-mesh disk of diameter 12 mm. Na metal was used as the negative electrode. Electrodes were separated by one layer of Whatman glass-fiber separator. Electrochemical data were collected by using a TOSCAT-3100 battery tester at C/20 rate [complete theoretical (dis)charge achieved in 20 h].

Mössbauer experiments were performed by using a Topologic System Inc. spectrometer, using a ^{57}Co source (Rh matrix) in transmission geometry. The velocity was calibrated by using pure α-Fe as a reference. Model fittings were performed with MossWinn 3.0 software. The electrochemically prepared samples were cycled in Na cells whose preparation is detailed above. After reaching the desired state, the voltage was maintained until the residual current dropped to 0 mA or was stable. The cells were then recovered in an inert atmosphere (Ar) and the electrodes were washed with dimethylcarbonate.

X-ray absorption near-edge structure (XANES) experiments were carried out at beamline 7C at the Photon Factory by the High-Energy Accelerator Research Organization (KEK). A Si(111) double-crystal monochromator was used for energy selection. The Fe and Mn absorption spectra were collected in the 6502–6610 eV (Mn *K*-edge) and 7076–7181 eV (Fe *K*-edge) energy ranges in transmission mode at room temperature. The intensities of incident and transmitted X-rays were monitored by using ionization chambers.

Acknowledgements

This work was supported by the Ministry of Education, Culture, Sports, Science, and Technology (MEXT), Japan, under the "Elemental Strategy Initiative for Catalysis and Batteries" (ESICB) project.

Keywords: alluaudite · high-voltage cathodes · iron sulfate · manganese sulfate · sodium-ion batteries

[1] R. L. Parker, *Composition of the Earth's Crust in Data of Geochemistry*, 6th ed., Ed. M. Fleischer, US Department of the Interior, Washington DC, **1924**.

[2] a) F. Sagane, T. Abe, Y. Iriyama, Z. Ogumi, *J. Power Sources* **2005**, *146*, 749–752; b) M. Okoshi, Y. Yamada, A. Yamada, H. Nakai, *J. Electrochem. Soc.* **2013**, *160*, A2160–A2165.

[3] N. Yabuuchi, M. Kajiyama, J. Iwatate, H. Nishikawa, S. Hitomi, R. Okuyama, R. Usui, Y. Yamada, S. Komaba, *Nat. Mater.* **2012**, *11*, 512–517.

[4] a) K. Trad, D. Carlier, L. Croguennec, A. Wattiaux, L. Besma, M. Ben Amara, C. Delmas, *J. Phys. Chem. C* **2010**, *114*, 10034–10044; b) M. Casas-Cabanas, V. V. Roddatis, D. Saurel, P. Kubiak, J. Carretero-González, V. Palomares, P. Serras, T. Rojo, *J. Mater. Chem.* **2012**, *22*, 17421–17423; c) P. Moreau, D. Guyomard, J. Gaubicher, F. Boucher, *Chem. Mater.* **2010**, *22*, 4126–4128.

[5] a) P. Barpanda, T. Ye, M. Avdeev, S.-C. Chung, A. Yamada, *J. Mater. Chem. A* **2013**, *1*, 4194–4197; b) P. Barpanda, T. Ye, S.-i. Nishimura, S.-C. Chung, Y. Yamada, M. Okubo, H. Zhou, A. Yamada, *Electrochem. Commun.* **2012**, *24*, 116–119.

[6] a) M. Bianchini, N. Brisset, F. Fauth, F. Weill, E. Elkaim, E. Suard, C. Masquelier, L. Croguennec, *Chem. Mater.* **2014**, *26*, 4238–4247; b) K. Chihara, A. Kitajou, I. D. Gocheva, S. Okada, J.-i. Yamaki, *J. Power Sources* **2013**, *227*, 80–85.

[7] a) J. M. Clark, C. Eames, M. Reynaud, G. Rousse, J.-N. Chotard, J.-M. Tarascon, M. S. Islam, *J. Mater. Chem. A* **2014**, *2*, 7446–7453; b) L. Lander, M. Reynaud, G. Rousse, M. T. Sougrati, C. Laberty-Robert, R. J. Messinger, M. Deschamps, J.-M. Tarascon, *Chem. Mater.* **2014**, *26*, 4178–4189; c) M. Reynaud, G. Rousse, A. M. Abakumov, M. T. Sougrati, G. Van Tendeloo, J.-N. Chotard, J.-M. Tarascon, *J. Mater. Chem. A* **2014**, *2*, 2671–2680.

[8] P. Barpanda, G. Oyama, C. D. Ling, A. Yamada, *Chem. Mater.* **2014**, *26*, 1297–1299.

[9] a) P. Barpanda, G. Oyama, S. Nishimura, S. C. Chung, A. Yamada, *Nat. Commun.* **2014**, *5*, 4358; b) J. Ming, P. Barpanda, S.-i. Nishimura, M. Okubo, A. Yamada, *Electrochem. Commun.* **2015**, *51*, 19–22; c) G. Oyama, S.-i. Nishimura, Y. Suzuki, M. Okubo, A. Yamada, *ChemElectroChem.* **2015**, *2*, 1019–1023.

[10] N. Furuta, S.-i. Nishimura, P. Barpanda, A. Yamada, *Chem. Mater.* **2012**, *24*, 1055–1061.

[11] D. R. Lide, *Handbook of Chemistry and Physics*, 89th ed., CRC Press, Boca Raton, FL, **2009**.

[12] D. Dwibedi, R. B. Araujo, S. Chakraborty, P. P. Shanbogh, N. G. Sundaram, R. Ahuja, P. Barpanda, *J. Mater. Chem. A* **2015**, *3*, 18564–18571.

[13] a) F. Zhou, M. Cococcioni, K. Kang, G. Ceder, *Electrochem. Commun.* **2004**, *6*, 1144–1148; b) T. Ye, P. Barpanda, S.-i. Nishimura, N. Furuta, S.-C. Chung, A. Yamada, *Chem. Mater.* **2013**, *25*, 3623–3629.

[14] a) A. Bhide, J. Hofmann, A. K. Durr, J. Janek, P. Adelhelm, *Phys. Chem. Chem. Phys.* **2014**, *16*, 1987–1998; b) S. Komaba, T. Ishikawa, N. Yabuuchi, W. Murata, A. Ito, Y. Ohsawa, *ACS Appl. Mater. Interfaces* **2011**, *3*, 4165–4168; c) A. Ponrouch, E. Marchante, M. Courty, J. M. Tarascon, M. R. Palacín, *Energy Environ. Sci.* **2012**, *5*, 8572–8583; d) B. Mortemard de Boisse, J. H. Cheng, D. Carlier, M. Guignard, C. J. Pan, S. Bordere, D. Filimonov, C. Drathen, E. Suard, B. J. Hwang, A. Wattiaux, C. Delmas, *J. Mater. Chem. A* **2015**, *3*, 10976–10989.

Manuscript received: October 18, 2015
Accepted Article published: December 7, 2015
Final Article published: December 10, 2015